IEEE Access
Multidisciplinary | Rapid Review | Open Access Journal

Received May 27, 2019, accepted June 10, 2019, date of publication June 13, 2019, date of current version June 28, 2019.

Digital Object Identifier 10.1109/ACCESS.2019.2922663

A Hi-Bi Ultra-Sensitive Surface Plasmon Resonance Fiber Sensor

MD. SAIFUL ISLAM[1,2], (Member, IEEE), CRISTIANO M. B. CORDEIRO[2,3], JAKEYA SULTANA[1], RIFAT AHMMED AONI[4], (Member, IEEE), SHILUN FENG[5], RAJIB AHMED[6], (Member, IEEE), MOHSEN DORRAKI[1], (Member, IEEE), ALEX DINOVITSER[1], (Member, IEEE), BRIAN WAI-HIM NG[1], (Senior Member, IEEE), AND DEREK ABBOTT[1], (Fellow, IEEE)

[1]School of Electrical and Electronic Engineering, The University of Adelaide, Adelaide, SA 5005, Australia
[2]Institute for Photonics and Advanced Sensing (IPAS), The University of Adelaide, Adelaide, SA 5005, Australia
[3]Institute of Physics, University of Campinas, Campinas 13083-859, Brazil
[4]Nonlinear Physics Centre, Research School of Physics and Engineering, The Australian National University, Canberra, ACT 2601, Australia
[5]School of Biomedical Engineering, Faculty of Science and Engineering, Macquarie University, NSW 2109, Australia
[6]Bio-Acoustic MEMS in Medicine (BAMM) Laboratory, School of Medicine, Stanford University, Palo Alto, CA 94304, USA

Corresponding author: Md. Saiful Islam (mdsaiful.islam@adelaide.edu.au)

The work of C. M. B. Cordeiro was supported by the Sao Paulo Research Foundation-FAPESP under Grant 2018/10409 − 7.

ABSTRACT In this paper, a simple, miniature, and highly sensitive photonic crystal fiber (PCF)-based surface plasmon resonance (SPR) sensor is proposed. The target analyte and the plasmonic material are at the outer surface of the fiber making practical applications feasible. A 30-nm gold (Au) layer supports surface plasmons. A thin titanium dioxide (TiO_2) layer is used to assist adhesion of Au on the glass fiber. The fiber cross section is formed purely by circular-shaped holes simplifying the preform manufacturing process. A high-birefringence (hi-bi) fiber is obtained by means of an array of air holes at the center of the fiber. A finite element method (FEM) is employed to analyze the surface plasmon properties of the proposed PCF-SPR sensor. By optimizing the geometric parameters, a maximum wavelength sensitivity (WS) of 25 000 nm/RIU and an amplitude sensitivity (AS) of 1411 RIU^{-1} for a dielectric refractive index (RI) range of 1.33–1.38 are obtained. Moreover, an estimated maximum resolution of 4×10^{-6} and a figure of merit (FOM) of 502 are obtained that ensures high detection accuracy of small refractive index (RI) changes. Owing to its sensitivity and simple architecture, the proposed sensor has potential application in a range of sensing application, including biosensing.

INDEX TERMS Surface plasmons, polarization, birefringence, resonance, plasmonics, optical sensing, sensors and actuators.

I. INTRODUCTION

Surface plasmon resonance (SPR) is a phenomenon that occurs when the frequency of incoming photons match the frequency of surface electrons. A slight change in surrounding RI potentially changes the effective RI experienced by the surface plasmon polariton (SPP) mode causing a shift of resonance wavelength and the unknown dielectric can be detected by observing the resonance peak shift. Note that the exploitation of SPR is advantageous for optical sensing because of its effectiveness, real-time detection and convenient operation [1], [2]. Notably, SPR technology is promising for applications in food safety, security, medical testing, biomolecular analyte detection, and medical diagnostics [2], [3].

In recent years, SPR modes supported by PCF have gained significant attention due to (i) the freedom to adjust optical parameters, by design, through the geometry of the structure, (ii) light weight, and (iii) controllable birefringence, making it ideal for a range of sensing applications [4]–[9]. Various optical fiber based RI sensing methods have been reported in the literature that include fiber Bragg grating (FBGs) [10]–[12], long period fiber gratings (LPFGs) [13], and modal interferometers [14] etc. Chryssis *et al.* [11] reported a RI sensor with an etched FBG, while in order to increase the sensitivity to environmental RI's the same etching process can also be applied to LPFGs [13]. Modal interferometers using tapered single

The associate editor coordinating the review of this manuscript and approving it for publication was Mauro Fadda.

mode fiber and based on core diameter mismatch provide new sensing opportunities [14], [15]. However, most of the reported sensors provide low sensitivity [27].

With the development of nanotechnology, several ways of improving the sensing performance of conventional SPR sensing techniques have emerged. One of the key strategies is the use of gold or silver nano particles with a diameter in the range of several tens nanometers or smaller where free electrons are trapped on a nanoparticle surface [16]. Under proper optical excitation these free electrons can oscillate collectively, and this results in localized SPR (LSPR). Note that, like SPR, LSPR is also sensitive to the change in the localized dielectric medium [17]. However, in addition to metallic nanoparticles recent advancements have shown other choices for sensitivity enhancement. The choices are quantum dots (QDs), graphene, hydrogel, magnetic and silicon nanoparticles and in most of the cases the sensitivity enhancement can be carried out using analyte enrichment. Recent reports show that plasmonic nanostructured arrays can also be used as a technique to improve the sensing performance [18], [19].

Utilizing the properties of PCF and different plasmonic materials, research has been carried out for SPR sensing. Generally, there are two types of SPR sensing approaches; (i) internal sensing and (ii) external sensing. In the internal sensing approach, the metal coating and dielectric fluid are placed inside the fiber. For example, this can be achieved by selectively filling air holes with the dielectric liquid to be analyzed. Using this internal sensing approach Shuai *et al.* designed a sensor with multi-analyte coating fiber and achieved a maximum negative sensitivity of $-5,500$ nm/RIU [20]. Later, Xue *et al.* proposed a Au coated fiber where the dielectric and metallic channel were considered inside the surface [21]. Moreover, Gao *et al.* proposed a TiO_2 coating based fiber that also fails to improve the sensing performance [22]. Recently, Rifat *et al.* [23] improved the sensitivity using the internal sensing approach. However, fabrication of this PCF is difficult due to (i) the need for internal metal coating and (ii) the requirement for filling the small air holes with the target dielectric [24]. Moreover, refilling and emptying of selected air holes is quite difficult and time consuming and thus the internal sensing approach is not feasible for real-time sensing [25].

Note that a PCF with a D-shaped structure provides a possible solution to internal sensing as the metallic and dielectric channels can be placed on the flat surface of the fiber and in direct contact with the external medium. A numerical study of D-shaped structure shows that the flat surface achieves high sensitivity [26], [28], [29]. A numerical study on dual sided polished fiber is also reported [30]. An experimental study on a side-polished structure shows a high wavelength sensitivity of 21, 700 nm/RIU with the RI range of 1.33 to 1.34. Although the cleaning of a D-shaped PCF is advantageous for refilling with the dielectric liquid, the standard surface polishing and etching of particular parts of a micro-structured PCF are challenging in practice [9], [26].

Considering the limitations of the internal sensing mechanism and sensing with a side polished PCF, external sensing is attractive as an approach for practical applications. In an external sensing, the dielectric fluid is placed in contact with the outer metallic layer of the PCF, that facilitates the cleaning and re-use of the fiber sensor with subsequent dielectrics. Therefore, considering external sensing, Dash *et al.* proposed a graphene-coated fiber and achieved a maximum WS and AS of 5, 000 nm/RIU and 860 RIU^{-1} respectively [31]. For further improvement, we propose a rectangular core gold coated SPR sensor that can achieve improved sensing performance, however achieving a rectangular shaped core is inconvenient for fabrication [33]. A spiral-shaped PCF has also been proposed but failed to improve the sensing performance [32]. Liu *et al.* proposed a gold-coated fiber that achieves a maximum WS of 15, 180 nm/RIU, however, due to large loss peak broadening they obtained a low AS of 498 RIU^{-1} [34].

In this manuscript, we propose a highly birefringent PCF-SPR sensor where the detection of unknown dielectrics can be carried out externally. The aim is to achieve improved WS and AS with high sensor resolution, long sensor length and high FOM. The simplicity in design enables a fabrication feasible PCF that opens the opportunity to commercial utilization of the sensor.

II. MODELING AND THEORETICAL ANALYSIS OF THE SENSOR

The modeling and numerical analysis is carried out using commercially available software COMSOL 5.3*a* where the *Wave Optics* module with the *Electromagnetic Waves, Frequency Domain* (EWFD) solver is used to investigate the guided response. The *Physics Controlled Mesh* sequence with *Extremely Fine* element size were used to obtain the best accuracy in numerical simulations where the structure subdivides into 229, 042 number of elements with minimum element quality of 0.7081, average element quality of 0.9618, element area ratio of 4.274×10^{-4}, and mesh area of 116 μm^2. For meshing the Au layer we use the *resolve wave in lossy media* function of COMSOL where Au is meshed in free space with a maximum mesh element size and that ensures simulation accuracy. The mesh characteristics of the Au layer are as follows, the number of vertices $=$ 16, 332, number of elements $=$ 27, 220, maximum element size $=$ 0.122 μm, minimum element quality $=$ 0.8537, Average element quality $=$ 0.951, and mesh area $=$ 0.6715 μm^2. Note that, the proposed model converged with the defined mesh property.

We use silica (SiO_2) glass as the bulk material whose RI profile can be obtained from the Sellmeier equation [35],

$$n = \sqrt{1 + \frac{0.696\lambda^2}{\lambda^2 - 0.0047} + \frac{0.408\lambda^2}{\lambda^2 - 0.014} + \frac{0.897\lambda^2}{\lambda^2 - 97.934}} \tag{1}$$

where λ stands for the wavelength of light. Note that, Eqn. 1 is valid for the wavelength region of 0.22 to 3.71 μm [35].

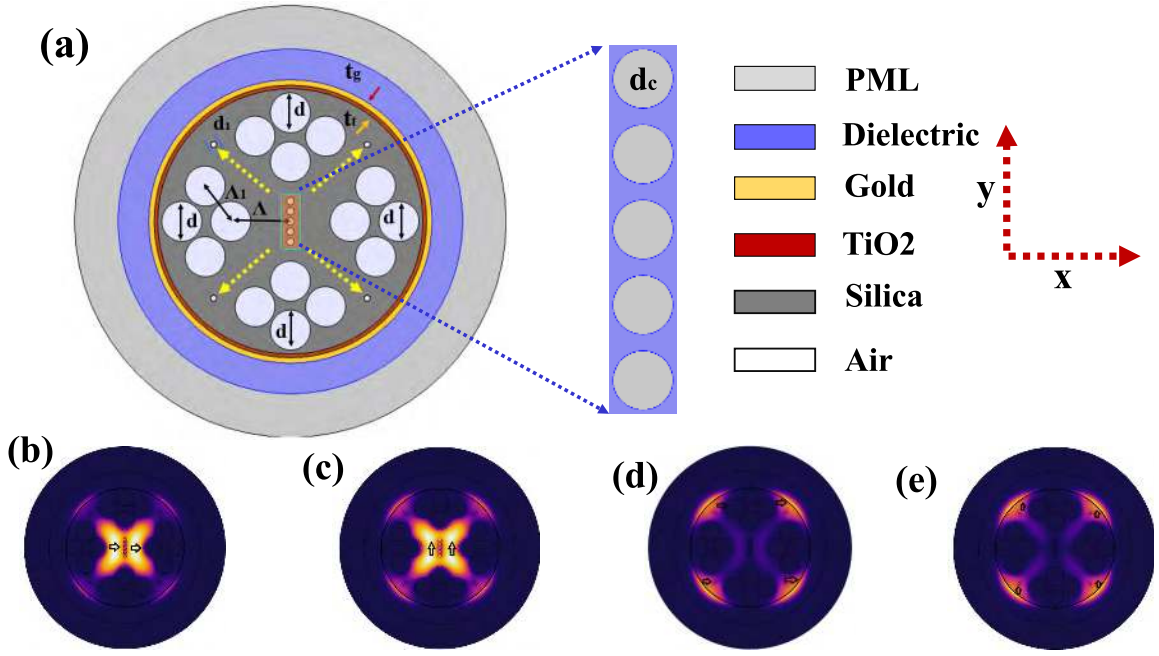

FIGURE 1. (a) Schematic cross section of the proposed PCF-SPR sensor with an enlarged view of the core where the yellow arrows indicate the direction of coupling of the core mode with the plasmonic mode; the optical field distribution at fundamental core mode (b) *x*-pol., (c) *y*-pol., and SPP mode at (d) *x*-pol., (e) *y*-pol. at an dielectric RI of 1.36 with resonance wavelength of 0.77 μm for *x*-pol. and 0.79 μm for *y*-pol.

At the center of the SiO_2 fiber an array of air holes of diameter d_c are used. The function of these air holes is to deflect the electromagnetic (EM) wave from the center towards the metal so that a strong plasmonic effect can be created. These also helps to create birefringence via an asymmetry required for maintaining the polarization modes. Although it is possible to create birefringence using a rectangular or an elliptical shaped air hole in the core, this is at the cost of increased fabrication complexity.

The cladding is based on circular shaped air holes of diameters d, and d_1. Arrangement of air holes having diameter d is carried out in such a way so that these can force the EM field to interact strongly with the metal. This facilitates a strong plasmonic effect in the created interaction channels (the created channels with the help of air holes of diameter d are shown by dotted yellow arrows in Fig. 1(a)). Here, four air holes of diameter d_1 are also placed on the way of the interaction channels that helps to reduce the confinement loss (CL) significantly. The E-field distribution of the proposed PCF-SPR for both x and y polarization is shown in Fig. 1(b), 1(c), 1(d) and 1(e). It can be observed that light is well confined in the core for both the polarization and interacts strongly with the plasmonic mode. The strong plasmonic property is an indication of achieving high WS and AS.

In contrast to previously reported PCFs [31], [32], [34] highlighted in Tab. 2, the proposed sensor is novel in the sense that it creates birefringence by creating asymmetry at the center of the fiber, creates four distinct channels for light interaction with the plasmonic metal, uses an additional layer (TiO_2) to support Au and improves the sensing performance over a large scale.

There are several materials such as gold (Au), silver (Ag), aluminium (Al), copper (Cu), indium tin oxide (ITO), and titanium nitride (TiN) that can be used to support surface plasmons in the optical frequency range. Among them, Au and Ag are widely used because of their relatively low loss in the visible to near-infrared [36]. The Ag gives rise to a sharper resonance peak compared to Au, however, when placed in a humid environment it becomes oxidized and this reduces the analyte detection accuracy [37]. On the other hand, Au is chemically stable, bio-compatible, and gives rise to a larger shift in the resonance wavelength. However, for very thin Au layers it experiences island growth and may flake off from the glass fiber. The material dispersion of gold can be characterized by the Drude-Lorentz model [38],

$$\varepsilon_m = \varepsilon_\infty - \frac{\omega_D^2}{\omega(\omega + j\gamma_D)} + \frac{\Delta_\varepsilon . \Omega_L^2}{(\omega^2 - \Omega_L^2) - j\Gamma_L \omega} \qquad (2)$$

where $\varepsilon_\infty = 5.9673$, $\Delta_\varepsilon = 1.09$ denotes the permittivity and the weighting vector respectively, ω represents the angular frequency, ω_D is defined as the plasma frequency and γ_D represents the damping frequency, where $\omega_D/2\pi = 2113.6$ THz, and $\gamma_D/2\pi = 15.92$ THz. Moreover, Ω_L and Γ_L indicate the frequency and spectral width of the Lorentz oscillator where $\Omega_L/2\pi = 650.07$ THz and $\Gamma_L/2\pi = 104.86$ THz [38].

To solve the adhesion problem of Au, a thin TiO_2 layer that has high RI having the features of non-toxicity and environmental compatibility is frequently used in between Au and glass. The deposition of TiO_2 thin film also increases

the surface plasmonic excitation that generate enhanced evanescent field. These create enhanced interaction of surface plasmons with its contacting dielectric, improves the sensitivity. This is because the TiO_2 has a high refractive index than the fiber itself. Therefore when a thin film of TiO_2 is placed on the glass surface it strongly attract the field from the core guided mode and strong coupling is created between the core guided and the plasmonic mode [26], [27]. Note that, there are multiple anisotropic microcrystallite rutile and sphalerite phases of TiO_2, with very high refractive index, and an amorphous phase with varying degrees of density [39]. Both the phases have different refractive index profiles that must be considered during an experiment. However, as this is a simulation study, we therefore use a generalized form of isotropic TiO_2 whose refractive index profile can be obtained from the following equation [40],

$$n_t = \sqrt{5.913 + \frac{2.441 \times 10^7}{\lambda^2 - 0.803 \times 10^7}} \tag{3}$$

where, n_t denotes the RI of TiO_2 and λ is in Angstroms.

At the Au surface we consider a dielectric layer where an analyte of particular refractive index (n_a) can be placed. Note that we consider the dielectric layer in contact with the outer surface so that filling and cleaning of analytes can be carried out easily. As this is a simulation study therefore the Au surface is not functionalized hence the surrounding of the sensor is homogeneous and has the refractive index of n_a. Therefore, the thickness of dielectric layer does not have any impact on the sensing performance, however, for simulation purposes we consider a constant dielectric thickness of 2.0 μm. As surface plasmons are extremely sensitive to the change of environmental RI, changes in local RI on the plasmonic metal surface can be determined by observing the changes of resonance wavelength, phase or intensity [41]. We vary the dielectric RI on the surface and observe the sensing performance. Note that this method of considering the analyte layer and method of calculating the sensitivity follows the standard approach in a number of references [3], [9], [10], [17], [23], [26], [30], [32], [25], [48]–[51], [30].

A mathematical boundary condition, i.e. a perfectly matched layer (PML), which by definition absorbs any energy that might be radiated, is added at the outer surface of the computational region. Note that there is no physical existence of the PML in practice, however, convenient to use in order to make the computation region finite [53]. The optical properties of the PML are similar to the dielectric and therefore PML thickness also has no impact on the overall sensing performance. However, for simulation purposes we consider a PML thickness similar to the dielectric thickness.

The proposed sensor is feasible for fabrication as it contains only circular shaped air holes. The different size of air holes can be realized using the standard stack-and-draw method [42], [43]. Drilling in the preform stage is also a possible route to create the holes and fabricate the fiber [44]. The thin Au and TiO_2 layer can be achieved using chemical vapor deposition (CVD), high-pressure microfluidic chemical deposition and wheel polishing methods [45].

The performance evaluation of the sensor is carried out using the resonance peak shift of the CL spectra that can be obtained from the following equation [8], [46],

$$\alpha_{loss} = 8.686 \times \frac{2\pi}{\lambda} \times \mathrm{Im}(n_{eff}) \times 10^4, \quad \mathrm{dB/cm} \tag{4}$$

where λ indicate the operating wavelength in microns, and Im (n_{eff}) represents the imaginary part of the complex RI of the core guided mode.

The sensitivity of a sensor can be determined using both the wavelength and amplitude interrogation technique. According to the wavelength interrogation method the WS of a sensor can be calculated by [47]

$$S_W(\lambda) = \frac{\Delta\lambda_{peak}}{\Delta n_a}, \tag{5}$$

where, $\Delta\lambda_{peak}$ denotes the wavelength difference between the loss peak shift and Δn_a indicates the change in dielectric RI.

The other sensing measurement method known as AS can be determined using the amplitude interrogation method [52],

$$S_A(\lambda) = -\frac{1}{\alpha(\lambda, n_a)} \frac{\delta\alpha(\lambda, n_a)}{\delta n_a} \tag{6}$$

where $\alpha(\lambda, n_a)$ is the overall loss where the dielectric RI is equal to n_a, $\delta\alpha(\lambda, n_a)$ represents the difference between two consecutive loss spectra due to a change of dielectric RI, and δn_a indicates the change in dielectric RI.

Besides the high sensitivity of a sensor, the length of the metal covered fiber is also an important property. Considering the input power launched into the fiber is P_0, the detected power at the output can be obtained by the following expression [6]

$$P(L, \lambda, n_a) = P_0 e^{-\alpha(\lambda, n_a)L} \tag{7}$$

where $\alpha(\lambda, n_a)$ is the attenuation constant and can be defined by Eqn. 4, L indicates the sensing length that can be defined by

$$L = \frac{1}{\alpha(\lambda, n_a)}. \tag{8}$$

The goal of this work is to propose a fiber design based solely on circular holes and whose metal layers are in the external interface of the waveguide. The fiber also needs to be highly birefringent in order to allow the transmitted signal to keep its linear polarization state along all fiber length. Denoting n_x and n_y the effective refractive indices of x and y polarization, the birefringence can be calculated as

$$B = n_x - n_y. \tag{9}$$

Sensor resolution that depends on the WS/AS determines the degree of dielectric RI detection. It can be determined by the following equation [55],

$$R = \frac{\Delta n_a \Delta\lambda_{min}}{\Delta\lambda_{peak}} \tag{10}$$

where, Δn_a represents a change in dielectric RI, $\Delta\lambda_{min}$ defines the estimated minimum wavelength resolution, and $\Delta\lambda_{peak}$ determines the difference in resonance peak shift.

III. INVESTIGATION OF SENSOR PERFORMANCE

The performance analysis of the proposed sensor is carried out by optimizing different geometrical parameters that include Au film thickness t_g, TiO_2 film thickness t_t, air hole diameters d and d_1, and number of core air holes n_c.

A. OPTIMIZATION OF FILM THICKNESS

Our simulations focused on the visible - near infrared region and the sensor performance was evaluated from 0.5 to 1.2 μm. Initially we tuned the geometrical parameters of the PCF and obtained an improved sensing performance with $d_c = 0.125\Lambda$, $d = 0.67\Lambda$, $d_1 = 0.09\Lambda$, $\Lambda = 1.65$ μm, $\Lambda_1 = 1.16$ μm, $n_c = 5$, $t_g = 30$ nm, and $t_t = 5$ nm. However, to show the performance variation with different parameter we first vary the t_t thickness while keeping the other parameters constant. The effect is shown in Fig. 2(a-b), where it can be seen that without TiO_2 the CL is relatively low, however, the WS and AS are also low. As the t_t increases the CL also increases and resonance peak shifts towards longer wavelengths. For $t_t = 10$ nm the CL is higher than $t_t = 0$ nm and $t_t = 5$ nm, moreover the loss peak broadens that results a low AS than experienced with $t_t = 5$ nm. Therefore, considering the loss peak broadening, WS and AS we choose $t_t = 5$ nm as optimum. It is well known that the Au film thickness t_g has a sharp impact on the CL, resonance peak shift and sensing performance of a fiber SPR sensor. Therefore, to investigate the effect of Au on the sensing performance we varied t_g and kept other parameters constant. The performance of the sensor with t_g variation is shown in Fig. 2(c-d) which indicate that increasing t_g increases the CL and shifts the resonance peak towards longer wavelengths by means of broadening the loss peak (Fig. 2(c)). Using $t_g = 40$ nm drastically reduces the AS Fig. 2(d) and induces a high loss reducing the maximum length of the fiber that could be metal coated—this is not desirable for a practical implementation. For $t_g = 20$ nm, the CL is low, however, that comes with a lower AS (970 RIU^{-1}) than $t_g = 30$ nm (1, 412 RIU^{-1}). Moreover, the WS at $t_g = 30$ nm is greater (9,000, nm/RIU) than $t_g = 20$ nm (4,000, nm/RIU). Therefore, we consider 30 nm as optimum Au thickness.

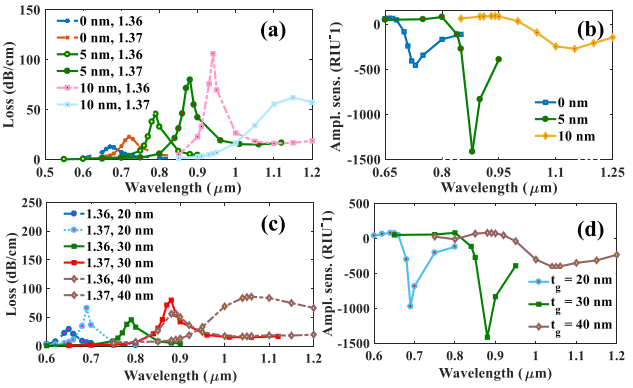

FIGURE 2. CL, for RI of 1.36 and 1.37, and AS (for 1.36), for the variation of TiO_2 thickness where t_g kept fixed at 30 nm (a-b); and for the variation of Au thickness where t_t kept fixed at 5 nm (c-d).

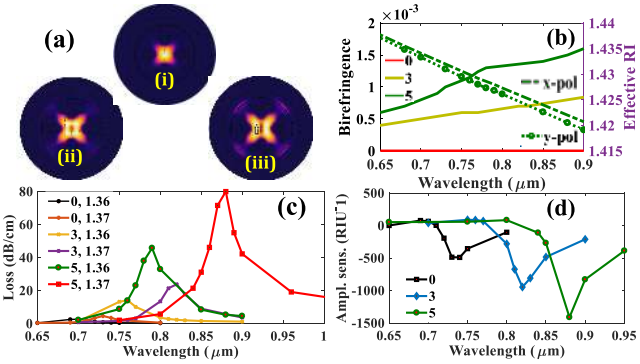

FIGURE 3. Optical field distribution at fundamental core mode having (i) solid core where $n_c = 0$, (ii) changing $n_c = 3$, and (iii) $n_c = 5$ (a); birefringence having $n_c = 0, 3, 5$, and effective RI of x and y-pol for an analyte RI of 1.36 (b), CL for an analyte RI of 1.36 and 1.37 (c), and AS for an analyte RI of 1.36 (d), having $n_c = 0, 3$, and 5.

B. EFFECT OF CORE AIR HOLES ON BIREFRINGENCE AND SENSING PERFORMANCE

The number of air holes in the core (n_c) has significant impact on the CL and overall sensitivity of the PCF-SPR sensor. Therefore, we observe the effect of solid core as well as core with different number of air holes. At optimized TiO_2 and Au thickness ($t_t = 5$ nm and $t_g = 30$ nm) with other constant values, the obtained electric field distribution having solid core, core with three air holes and core with five air holes is shown in Fig. 3(a). It is observable that the EM field within a solid core has low interaction with the surface whereas maximum interaction is obtained with a core possessing five air holes. It can be seen that, with solid core, the sensor experiences negligible CL (Fig. 3(c)), however, that comes with low sensitivity (Fig. 3(d)) and undesirable close to zero birefringence (Fig. 3(b)). Note that birefringence is an important property of a fiber based plasmonic sensor as it will lead to a differential sensitivity between x- and y-polarized signals. More importantly, the input signal lunched on the fiber axis will keep its polarization state along the fiber [31]–[34], [6].

Moreover, a birefringent fiber is required for signal detection which is based on lunching polarized broadband light in one of the fiber polarization axes while detecting the transmitted signal in a fiber spectrometer. By characterizing the wavelength and amplitude shift of the transmitted spectrum, and using previously measured data, the RI of the fluid that baths the fiber can be characterized.

With $n_c = 3$ we can see that the sensitivity increases over that of a solid core, however, maximum WS and AS with high birefringence is obtained having $n_c = 5$. Therefore, we consider $n_c = 5$ as optimum of our designed sensor. We can see the fiber birefringence increases with the wavelength. This behavior is related with the fact that longer

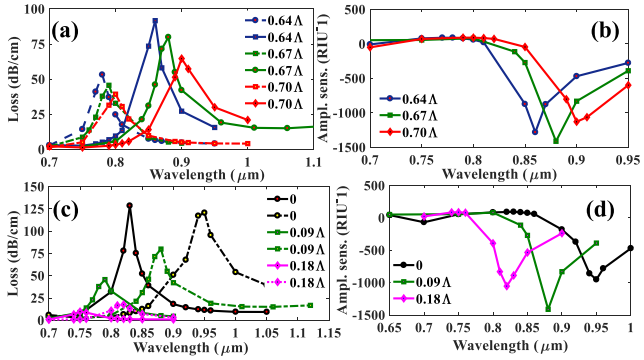

FIGURE 4. CL having RI's of 1.36 (dashed line), 1.37 (solid line) and AS (1.36) on the variation of d, (a-b); and CL having RI's of 1.36 (solid line), 1.37 (dashed line) and AS (1.36) on the variation of d_1, (c-d).

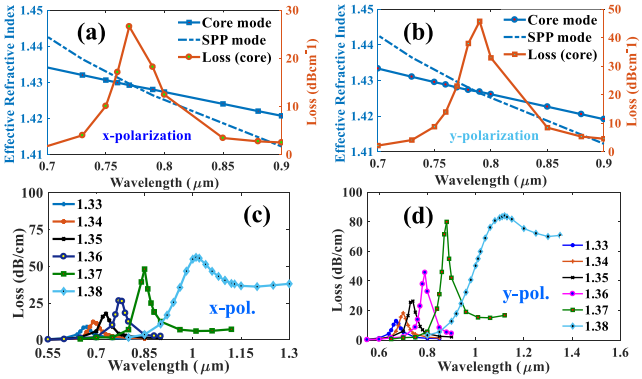

FIGURE 5. The wavelength dependent dispersion relation of the proposed sensor at fundamental core mode, SPP mode and loss spectra for an dielectric RI $n_a = 1.36$ at (a) x-pol, (b) y pol.; CL at optimized geometrical parameters including the metal thickness for (c) x-pol., and (d) y-pol.

wavelengths spread more within the fiber cross section being more influenced by the asymmetric holes distribution. Note that, we also investigate the sensor performance at $n_c = 1$, however, we do not consider that as optimum because it creates zero birefringence with low sensitivity.

Note that the coupling between the fiber core mode and the plasmonic mode depends on the polarization of optical signal that reaches the coated region of the fiber. The device response can be analyzed with the help of Fig. 5 (a-d) where it can noted the phase-matching wavelength and coupling strength (in practical terms, the induced loss) depend on the polarizing state of the guided mode (x or y direction). To obtain a sensing device with a reproducible and predictable response this phase matching should be as independent as possible of external spurious influences as fiber bending, temperature variations etc. The use of a single mode hi-bi fiber helps to address this issue. In our proposed design we reached such situation with a microstructured optical fiber whose cross section is formed just by circular holes, turning its fabrication feasible via the well-known stacking-and-draw technique [43] or by directly drilling the holes on the fiber preform stage [44].

Our fiber is, in practical terms, single mode as the first higher order mode presents a CL that is 1.37 times bigger than the fundamental core mode. The fiber is also highly birefringence ($B \sim 10^{-3}$) when we add the central holes in the core area—see Fig. 3 (b). This means that any linearly polarized light that is lunched on the x or y axis of the fiber will keep this polarization stage along the fiber length, independently of external mechanical and thermal perturbations the fiber may suffer.

By choosing between lunching the input signal in the y or x axes we can select between improving the fiber sensitivity (y-axis) or reducing the loss (x-axis) what can lead to longer metal coated sections.

C. EFFECT OF CLADDING AIR HOLES D AND D_1

The effect of cladding air holes of diameter d is shown in Fig. 4 (a) and 4 (b). We can see that, higher CL is obtained at $d = 0.64\Lambda$ and lower AS is obtained at $d = 0.70\Lambda$. However, moderate CL and highest sensitivity are obtained at 0.67Λ therefore we choose 0.67Λ as optimum for d.

The air holes d_1 at four corners have also significant impact on CL and overall sensing performance of the sensor. Therefore we investigated the performance of the sensor with and without d_1 that is shown in Fig. 4 (c-d). It can be seen that without d_1 the sensor experiences a high CL that also comes with a low wavelength and AS as compared to the fiber having d_1. This is because, without d_1 the EM fields from the core scattered largely towards the metal therefore creates high CL with loss peak broadening, however, placing air holes at four corners limits scattering and therefore reduce the loss. Hence we decided to keep air holes at four corners, however, with optimized diameter. Note that, we cannot make $d_1 = d$ because that will prevent the EM fields from passing through and interacting with the metal to create an evanescent wave. Therefore we varied d_1 and found $d_1 = 0.18\Lambda$ shows low CL, however, $d_1 = 0.09\Lambda$ shows improved sensing performance. Therefore, we choose $d_1 = 0.09\Lambda$ as the optimum diameter of the corner air holes.

D. DISPERSION RELATION AND OPTIMIZED SENSOR PERFORMANCE

The dispersion relation of the proposed sensor for a dielectric RI of 1.36 is shown in Fig. 5(a-b). It can be seen that at the RI matching point of the core mode and SPP mode the CL reaches to its maximum. The higher loss is obtained at y-polarization than the loss in x-polarization as high penetration of electric field from the core towards the dielectric occurs at y-polarization.

Fig. 5(c-d) show the peak shift of absorption loss for a range of dielectric RI. Here, all the performance evaluation of the sensor is based on change of effective refractive index of the core guided mode. From Fig. 5(c) we can see that the loss peaks are obtained at 670, 690, 730, 770, 850, and 1,011 nm where the wavelength differences are 20, 40, 40, 80, and 161 nm respectively for dielectric RI range of 1.33–1.38. Similarly for the y-polarization, according to Fig. 5(d) the wavelength differences are 30, 40, 50, 90, and 250 nm respectively.

TABLE 1. Performance analysis of the proposed sensor by varying the dielectric RI adjacent to Au surface.

dielectric RI	Peak wavelength (nm)		Amplitude sensitivity (RIU^{-1})		Wavelength sensitivity (nm/RIU)		Figure of merit (FOM)	
	x-pol	y-pol	x-pol	y-pol	x-pol	y-pol	x-pol	y-pol
1.33	670	670	242	242	2,000	3,000	42	64
1.34	690	700	398	455	4,000	4,000	89	90
1.35	730	740	631	826	4,000	5,000	91	104
1.36	770	790	1311	1412	8,000	9,000	182	178
1.37	850	880	837	404	16,100	25,000	319	502
1.38	1011	1120	N/A	N/A	N/A	N/A	N/A	N/A

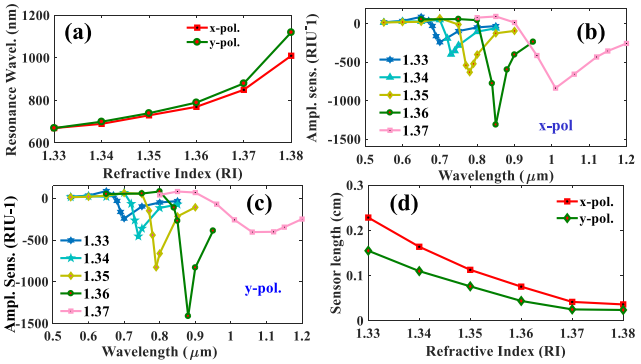

FIGURE 6. Resonance wavelength vs dielectric RI (a); AS for x-pol (b); AS for y-pol (c); and Sensing length (d), having $n_a = 1.33$–1.38 and for both x and y polarization mode.

In this study we focused on the refractive index range around water (1.33 to 1.37) due its possible application in real time analysis of samples with biological interest. The waveguide geometrical parameters and the metals thickness were optimized to this range as well. There are a number of biological agents and chemical solutions that have refractive index within the specified range (1.33-1.38) (for example, ethanol = 1.361, acetone = 1.36, 10% glucose solution in water = 1.3477, 20% Glucose solution in water = 1.3635, liver (human) = 1.369, intestinal mucosa (human) = 1.329-1.338) etc that the proposed sensor can detect. Note that the reported RI range is very similar to previously reported SPR sensors [31]–[34], [25], [48]–[50]. However, instead of using the name of dielectrics we used the relative refractive indices in order to generalize the discussion.

According to the wavelength interrogation method mentioned in Eqn. 5 the obtained WS's for the x polarization are 2,000, 4,000, 4,000, 8,000 and 16,000 nm/RIU while for the y-polarization the obtained sensitivities are 3,000, 4,000, 5,000, 9,000 and 25,000 nm/RIU for RI range of 1.33–1.37 respectively. In Fig. 6(a), we further show the change of resonance wavelength by means of dielectric RI from where the wavelength sensitivity can easily be calculated for x- and y- polarized signals.

Apart from WS, the sensing performance is also carried out using the amplitude interrogation (AI) method as mentioned in Eqn. 6. Note that, obtaining an AS is less complex than WS as it does not require spectrum monitoring, whereas dielectric detection is carried out for a particular wavelength [52]. Fig. 6(b-c) show the AS of the proposed sensor for both x and y polarization. We can see that with the increase of dielectric RI the AS increases upto $n_a = 1.36$ and then starts to decrease. This is because, a sharp loss peak is obtained up to $n_a = 1.37$ that then starts broadening thus the AS also begins to decrease.

The sensing length with different dielectric RI variation is shown in Fig. 6(d) that is derived from Eqn. 9. It indicates that as the dielectric RI increases the sensing length decreases because the length of a sensor is totally dependent on the absorption loss. According to the observation of Fig. 6(d) we can conclude that sensing length of a few millimeters to a centimeter can be used to detect dielectrics over a useful range of refractive indices.

According to Eqn. 10, for a best-case estimate considering $\Delta\lambda_{min} = 0.1$ nm, the proposed sensor shows high wavelength sensing resolution of 6.21×10^{-6} in the x polarization and 4×10^{-6} in the y polarization. Therefore, the proposed sensor can in principle detect a tiny change in RI of the order of 10^{-6}.

Another important metric known as the FOM characterizes the overall performance of a sensor that can be defined as a ratio of sensitivity to full width at half maximum (FWHM) (FOM = S_λ (nm/RIU)/FWHM (nm)) [30], [54]. A high performance sensor can be realized when the sensitivity increase and FWHM decrease. The FOM for different dielectrics of the proposed sensor is shown in Tab. 1 from where we can see that a maximum FOM of 319 is obtained for x-polarization and 502 is obtained for y-polarization. Note that, a larger FOM means a better detection limit [30].

The performance evaluation based on WS, AS and FOM with changing dielectric RI is shown in Tab. 1. It can be seen that, maximum AS of 1,311 and 1,412 RIU^{-1}, maximum WS of 16,100 and 25,000 nm/RIU, and maximum FOM of 319 and 502 are obtained for the x and y polarization's respectively. A detail performance analysis of the proposed sensor with the prior sensors that use external sensing approach is carried out and shown in Tab. 2. Comparing with the purely external (not side polished) sensing approach based sensors it can be seen that the proposed sensor shows improved

TABLE 2. Comparison of performance of the proposed sensor with prior sensors having practical sensing approach.

Ref.	Sensing Approach	RI Range	Birefringence	Max. Amp. Sens. (RIU^{-1})	Max. Wavel. Sens. (nm/RIU)	Sensor Resolution	FOM
[28]	External (side polished)	1.18–1.36	-	$1,054$	$20,000$	5×10^{-6}	-
[29]	External (side polished)	1.22–1.37	-	$1,872$	$51,000$	1.96×10^{-6}	566
[31]	External	1.33–1.37	-	860	$5,000$	4×10^{-5}	-
[32]	External	1.33–1.38	-	420.4	$4,600$	2.17×10^{-5}	-
[34]	External	1.40–1.43	-	498	$15,180$	5.68×10^{-6}	-
This paper	External	1.33–1.38	1.6×10^{-3}	$1,411$	$25,000$	4×10^{-6}	502

performance in consideration to wavelength sensitivity, AS, birefringence, sensor resolution and FOM.

IV. CONCLUSIONS

A simple Au-TiO_2 based PCF-SPR sensor is proposed and analyzed. Based on optimized structural parameters, proposed polarization sensitive sensor shows a relatively high AS of 1,411 RIU^{-1} and WS of 25,000 nm/RIU with high degree of detection limit. The proposed fiber design is also highly birefringent what potentially improves the sensing performance. Moreover, the sensor attains a high FOM that indicates the high overall sensing performance. The practical utilization of the sensor is simple as it utilizes an external sensing approach with only circular shaped air holes. The long length of the sensor is another attractive feature that in addition with suitable surface functionalization makes the proposed sensor promising for biosensing applications.

REFERENCES

[1] J. Homola, S. S. Yee, and G. Gauglitz, "Surface plasmon resonance sensors: Review," *Sens. Actuators B, Chem.*, vol. 54, nos. 1–2, pp. 3–15, 1999.

[2] L. G. Carrascosa, "Molecular inversion probe-based SPR biosensing for specific, label-free and real-time detection of regional DNA methylation," *Chem. Commun.*, vol. 50, no. 27, pp. 3585–3588, 2014.

[3] B. Lee, S. Roh, and J. Park, "Current status of micro-and nano-structured optical fiber sensors," *Opt. Fiber Technol.*, vol. 15, pp. 209–221, Jun. 2009.

[4] M. S. Islam, J. Sultana, K. Ahmed, M. R. Islam, A. Dinovitser, B. W.-H. Ng, and D. Abbott, "A novel approach for spectroscopic chemical identification using photonic crystal fiber in the terahertz regime," *IEEE Sensors J.*, vol. 18, no. 2, pp. 575–582, Jan. 2018.

[5] M. S. Islam, J. Sultana, A. A. Rifat, A. Dinovitser, B. W.-H. Ng, and D. Abbott, "Terahertz sensing in a hollow core photonic crystal fiber," *IEEE Sensors J.*, vol. 18, no. 10, pp. 4073–4080, May 2018.

[6] J. N. Dash and R. Jha, "Highly sensitive side-polished birefringent PCF-based SPR sensor in near IR," *Plasmonics*, vol. 11, no. 6, pp. 1505–1509, 2016.

[7] J. N. Dash and R. Das, "SPR based magnetic-field sensing in microchannelled PCF: A numerical approach," *J. Opt.*, vol. 20, no. 11, 2018, Art. no. 115001.

[8] J. N. Dash, R. Das, and R. Jha, "AZO coated microchannel incorporated PCF-based SPR sensor: A numerical analysis," *IEEE Photon. Technol. Lett.*, vol. 30, no. 11, pp. 1032–1035, Jun. 1, 2018.

[9] J. N. Dash and R. Jha, "On the performance of graphene-based D-shaped photonic crystal fibre biosensor using surface plasmon resonance," *Plasmonics*, vol. 10, no. 5, pp. 1123–1131, 2015.

[10] A. Iadicicco, A. Cusano, S. Campopiano, A. Cutolo, and M. Giordano, "Thinned fiber Bragg gratings as refractive index sensors," *IEEE Sensors J.*, vol. 5, no. 6, pp. 1288–1295, Dec. 2005.

[11] A. N. Chryssis, S. M. Lee, S. B. Lee, S. S. Saini, and M. Dagenais, "High sensitivity evanescent field fiber Bragg grating sensor," *IEEE Photon. Technol. Lett.*, vol. 17, no. 6, pp. 1253–1255, Jun. 2005.

[12] J. H. Osório, R. Oliveira, S. Aristilde, G. Chesini, M. A. R. Franco, R. N. Nogueira, and C. M. B. Cordeiro, "Bragg gratings in surface-core fibers: Refractive index and directional curvature sensing," *Opt. Fiber Technol.*, vol. 34, pp. 86–90, Mar. 2017.

[13] H. J. Patrick, A. D. Kersey, and F. Bucholtz, "Analysis of the response of long period fiber gratings to external index of refraction," *J. Lightw. Technol.*, vol. 16, no. 9, pp. 1606–1612, Sep. 1998.

[14] J. Zhou, Y. Wang, C. Liao, B. Sun, J. He, G. Yin, S. Liu, Z. Li, G. Wang, X. Zhong, and J. Zhao, "Intensity modulated refractive index sensor based on optical fiber Michelson interferometer," *Sens. Actuators B, Chem.*, vol. 208, pp. 315–319, Mar. 2015.

[15] M. I. Zibaii, H. Latifi, M. Karami, M. Gholami, S. M. Hosseini, and M. H. Ghezelayagh, "Non-adiabatic tapered optical fiber sensor for measuring the interaction between α-amino acids in aqueous carbohydrate solution," *Meas. Sci. Technol.*, vol. 21, no. 10, 2010, Art. no. 105801.

[16] Y. Zeng, R. Hu, L. Wang, D. Gu, J. He, S.-Y. Wu, H.-P. Ho, X. Li, J. Qu, B. Z. Gao, and Y. Shao, "Recent advances in surface plasmon resonance imaging: Detection speed, sensitivity, and portability," *Nanophotonics*, vol. 6, no. 5, pp. 1017–1030, 2017.

[17] G. A. Lopez, M.-C. Estevez, M. Soler, and L. M. Lechuga, "Recent advances in nanoplasmonic biosensors: Applications and lab-on-a-chip integration," *Nanophotonics*, vol. 6, no. 1, pp. 123–136, 2016.

[18] J. Jiang, X. Wang, S. Li, F. Ding, N. Li, S. Meng, R. Li, J. Qi, Q. Liu, and G. L. Liu, "Plasmonic nano-arrays for ultrasensitive bio-sensing," *Nanophotonics*, vol. 7, no. 9, pp. 1517–1531, 2018.

[19] Y.-F. C. Chau, C.-K. Wang, L. Shen, C. M. Lim, H.-P. Chiang, C.-T. C. Chao, H. J. Huang, C.-T. Lin, N. T. R. N. Kumara, and N. Y. Voo, "Simultaneous realization of high sensing sensitivity and tunability in plasmonic nanostructures arrays," *Sci. Rep.*, vol. 7, no. 1, p. 16817, 2017.

[20] B. Shuai, L. Xia, and D. Liu, "Coexistence of positive and negative refractive index sensitivity in the liquid-core photonic crystal fiber based plasmonic sensor," *Opt. Exp.*, vol. 20, no. 23, pp. 25858–25866, Nov. 2012.

[21] J. Xue, S. Li, Y. Xiao, W. Qin, X. Xin, and X. Zhu, "Polarization filter characters of the gold-coated and the liquid filled photonic crystal fiber based on surface plasmon resonance," *Opt. Express* vol. 21, no. 11, pp. 13733–13740, 2013.

[22] D. Gao, C. Guan, Y. Wen, X. Zhong, and L. Yuan, "Multi-hole fiber based surface plasmon resonance sensor operated at near-infrared wavelengths," *Opt. Commun.*, vol. 313, pp. 94–98, Feb. 2014.

[23] A. A. Rifat, F. Haider, R. Ahmed, G. A. Mahdiraji, F. R. M. Adikan, and A. E. Miroshnichenko, "Highly sensitive selectively coated photonic crystal fiber-based plasmonic sensor," *Opt. Lett.*, vol. 43, no. 4, pp. 891–894, 2018.

[24] A. A. Rifat, R. Ahmed, G. A. Mahdiraji, and F. M. Adikan, "Highly sensitive D-shaped photonic crystal fiber-based plasmonic biosensor in visible to near-IR," *IEEE Sensors J.*, vol. 17, no. 9, pp. 2776–2783, Jun. 2017.

[25] N. Luan, R. Wang, W. Lv, and J. Yao, "Surface plasmon resonance sensor based on D-shaped microstructured optical fiber with hollow core," *Opt. Express*, vol. 23, no. 7, pp. 8576–8582, Mar. 2015.

[26] A. A. Rifat, G. Mahdiraji, Y. M. Sua, R. Ahmed, Y. Shee, and F. M. Adikan, "Highly sensitive multi-core flat fiber surface plasmon resonance refractive index sensor," *Opt. Exp.*, vol. 24, no. 3, pp. 2485–2495, 2016.

[27] C.-L. Tien, H.-Y. Lin, and S.-H. Su, "High sensitivity refractive index sensor by D-shaped fibers and titanium dioxide nanofilm," *Adv. Condens. Matter Phys.*, vol. 2018, Feb. 2018, Art. no. 2303740.

[28] E. Haque, M. A. Hossain, F. Ahmed, and Y. Namihira, "Surface plasmon resonance sensor based on modified *D*-shaped photonic crystal fiber for wider range of refractive index detection," *IEEE Sensors J.*, vol. 18, no. 20, pp. 8287–8293, Oct. 2018.

[29] E. Haque, M. A. Hossain, Y. Namihira, and F. Ahmed, "Microchannel-based plasmonic refractive index sensor for low refractive index detection," *Appl. Opt.*, vol. 58, no. 6, pp. 1547–1554, 2019.

[30] C. Liu, W. Su, X. Lu, F. Wang, T. Sun, and P. K. Chu, "Symmetrical dual D-shape photonic crystal fibers for surface plasmon resonance sensing," *Opt. Express*, vol. 26, no. 7, pp. 9039–9049, 2018.

[31] J. N. Dash and R. Jha, "Graphene-based birefringent photonic crystal fiber sensor using surface plasmon resonance," *IEEE Photon. Technol. Lett.*, vol. 26, no. 11, pp. 1092–1095, Jun. 1, 2014.

[32] M. R. Hasan, S. Akter, A. A. Rifat, S. Rana, K. Ahmed, R. Ahmed, H. Subbaraman, and D. Abbott, "Spiral photonic crystal fiber-based dual-polarized surface plasmon resonance biosensor," *IEEE Sensors J.*, vol. 18, no. 1, pp. 133–140, Jan. 2018.

[33] M. S. Islam, J. Sultana, A. A. Rifat, R. Ahmed, A. Dinovitser, B. W.-H. Ng, H. Ebendorff-Heidepriem, and D. Abbott, "Dual-polarized highly sensitive plasmonic sensor in the visible to near-IR spectrum," *Opt. Express*, vol. 26, no. 23, pp. 30347–30361, 2018.

[34] M. Liu, X. Yang, P. Shum, and H. Yuan, "High-sensitivity birefringent and single-layer coating photonic crystal fiber biosensor based on surface plasmon resonance," *Appl. Opt.*, vol. 57, no. 8, pp. 1883–1886, 2018.

[35] I. H. Malitson, "Interspecimen comparison of the refractive index of fused silica," *J. Opt. Soc. Amer.*, vol. 55, no. 10, pp. 1205–1208, 1965.

[36] P. R. West, S. Ishii, G. V. Naik, N. Emani, V. M. Shalaev, and A. Boltasseva, "Searching for better plasmonic materials," *Laser Photon. Rev.*, vol. 4, no. 6, pp. 795–808, Nov. 2009.

[37] A. A. Rifat, G. A. Mahdiraji, D. M. Chow, Y. G. Shee, R. Ahmed, and F. R. M. Adikan, "Photonic crystal fiber-based surface plasmon resonance sensor with selective analyte channels and graphene-silver deposited core," *Sensors*, vol. 15, no. 5, pp. 11499–11510, 2015.

[38] A. Vial, A.-S. Grimault, D. Macías, D. Barchiesi, and M. L. de L. Chapelle, "Improved analytical fit of gold dispersion: Application to the modeling of extinction spectra with a finite-difference time-domain method," *Phys. Rev. B, Covering Condens. Matter Mater. Phys.*, vol. 71, Feb. 2005, Art. no. 085416.

[39] J. Kischkat, S. Peters, B. Gruska, M. Semtsiv, M. Chashnikova, M. Klinkmüller, O. Fedosenko, S. Machulik, A. Aleksandrova, G. Monastyrskyi, Y. Flores, and W. T. Masselink, "Mid-infrared optical properties of thin films of aluminum oxide, titanium dioxide, silicon dioxide, aluminum nitride, and silicon nitride," *Appl. Opt.*, vol. 51, no. 28, pp. 6789–6798, 2012.

[40] J. R. DeVore, "Refractive indices of rutile and sphalerite," *J. Opt. Soc. Amer.*, vol. 41, no. 6, pp. 416–419, 1951.

[41] B. Špačková, P. Wrobel, M. Bocková, and J. Homola, "Optical biosensors based on plasmonic nanostructures: A review," *Proc. IEEE*, vol. 104, no. 12, pp. 2380–2408, Dec. 2016.

[42] G. A. Mahdiraji, D. M. Chow, S. R. Sandoghchi, F. Amirkhan, E. Dermosesian, K. S. Yeo, Z. Kakaei, M. Ghomeishi, S. Y. Poh, S. Y. Gang, and F. R. M. Adikan, "Challenges and solutions in fabrication of silica-based photonic crystal fibers: An experimental study," *Fiber Integr. Opt.*, vol. 33, nos. 1–2, pp. 85–104, 2014.

[43] J. C. Knight, "Photonic crystal fibers," *Nature*, vol. 424, no. 6950, pp. 847–851, Jan. 2003.

[44] R. Kostecki, H. Ebendorff-Heidepriem, C. Davis, G. McAdam, S. C. Warren-Smith, and T. M. Monro, "Silica exposed-core microstructured optical fibers," *Opt. Mater. Express*, vol. 2, no. 11, pp. 1538–1547, 2012.

[45] X. Zhang, R. Wang, F. M. Cox, B. T. Kuhlmey, and M. C. J. Large, "Selective coating of holes in microstructured optical fiber and its application to in-fiber absorptive polarizers," *Opt. Express*, vol. 15, no. 24, pp. 16270–16278, Nov. 2007.

[46] D. Ying, L. Shu-Guang, and L. Shuo, "Wavelength-selective characteristics of high birefringence photonic crystal fiber with Au nanowires selectively filled in the cladding air holes," *Chin. Phys. B*, vol. 21, no. 9, 2012, Art. no. 094219.

[47] E. K. Akowuah, T. Gorman, H. Ademgil, S. Haxha, G. K. Robinson, and J. V. Oliver, "Numerical analysis of a photonic crystal fiber for biosensing applications," *IEEE J. Quantum Electron.*, vol. 48, no. 11, pp. 1403–1410, Nov. 2012.

[48] A. Aray, H. Saghafifar, and M. Soltanolkotabi, "Calculation of dispersion relation and single mode operation in surface plasmon resonance based fiber optic refractive index sensors," *J. Lightw. Technol.*, vol. 34, no. 11, pp. 2782–2788, Jun. 1, 2016.

[49] Z.-W. Ding, T.-T. Lang, Y. Wang, and C.-L. Zhao, "Surface plasmon resonance refractive index sensor based on tapered coreless optical fiber structure," *J. Lightw. Technol.*, vol. 35, no. 21, pp. 4734–4739, Nov. 1, 2017.

[50] S. Jiao, S. Gu, H. Yang, H. Fang, and S. Xu, "Highly sensitive dual-core photonic crystal fiber based on a surface plasmon resonance sensor with a silver nano-continuous grating," *Appl. Opt.*, vol. 57, no. 28, pp. 8350–8358, 2018.

[51] S. Chu, K. Nakkeeran, A. M. Abobaker, S. S. Aphale, P. R. Babu, and K. Senthilnathan, "Design and analysis of surface-plasmon-resonance-based photonic quasi-crystal fiber biosensor for high-refractive-index liquid analytes," *IEEE J. Sel. Topics Quantum Electron.*, vol. 25, no. 2, Mar./Apr. 2019, Art. no. 6900309.

[52] B. Gauvreau, A. Hassani, M. F. Fehri, A. Kabashin, and M. Skorobogatiy, "Photonic bandgap fiber-based surface plasmon resonance sensors," *Opt. Express*, vol. 15, no. 18, pp. 11413–11426, 2007.

[53] W. Shin and S. Fan, "Choice of the perfectly matched layer boundary condition for frequency-domain Maxwell's equations solvers," *J. Comput. Phys.*, vol. 231, no. 8, pp. 3406–3431, 2012.

[54] T. Srivastava, R. Das, and R. Jha, "Highly sensitive plasmonic temperature sensor based on photonic crystal surface plasmon waveguide," *Plasmonics*, vol. 8, no. 2, pp. 515–521, 2013.

[55] M. Hautakorpi, M. Mattinen, and H. Ludvigsen, "Surface-plasmon-resonance sensor based on three-hole microstructured optical fiber," *Opt. Express*, vol. 16, no. 12, pp. 8427–8432, Jun. 2008.

MD. SAIFUL ISLAM (M'18) is currently pursuing the Ph.D. degree with the School of Electrical and Electronic Engineering, The University of Adelaide, Australia. His research interests include optical fiber communication, PCF-based terahertz waveguides, terahertz sensors, surface plasmon resonance biosensors, topological insulators, and metamaterials for sensing applications. He has published 33 peer-reviewed articles and actively reviews for the IEEE JOURNAL OF LIGHTWAVE TECHNOLOGY, the IEEE PHOTONICS JOURNAL, the IEEE SENSORS JOURNAL, the IEEE PHOTONICS TECHNOLOGY LETTERS, *Optics Express*, *Applied Optics*, *Optical Materials Express*, and *Optical Fiber Technology*. He is a member of the IEEE Young Professionals, the Optical Society of America (OSA), and the Institute for Photonics & Advanced Sensing (IPAS).

CRISTIANO M. B. CORDEIRO received the Ph.D. degree from the University of Campinas (UNICAMP), Brazil. He did his postdoctoral research at the University of Bath, U.K. He is currently an Assistant Professor with the Institute of Physics, UNICAMP, and the Head of the Specialty Optical Fiber Laboratory. The main research areas of the laboratory are the development and application of silica photonic crystal fibers, microstructured polymer optical fibers, and micro/nanofibers. His research interests include exploring new fiber functionalities and the use of new technologies in the optical fiber area. Applications related with optical devices and fiber sensors are under investigation. He has authored 70 journal publications, 50 communications in international conferences, and a book chapter. He holds eight patents. He chaired the First Edition of the Workshop on Specialty Optical Fibers (WSOF), now in its Sixth Edition.

JAKEYA SULTANA received the B.Sc.Engg. degree from the Rajshahi University of Engineering & Technology and the M.Sc.Engg. degree from the Islamic University of Technology, Bangladesh, in 2014 and 2017, respectively. She is currently pursuing the Ph.D. degree with the School of Electrical and Electronic Engineering, The University of Adelaide, Australia. She is also an Active Reviewer of JOURNAL OF LIGHTWAVE TECHNOLOGY, the IEEE PHOTONICS TECHNOLOGY LETTER, *Optik*, and *Optics Communication*. Her research interests include anti-resonant fibers for terahertz application, and super-continuum generation.

RIFAT AHMMED AONI (M'18) is currently pursuing the Ph.D. degree with The Australian National University, Australia. He was a Research Assistant with the Integrated Lightwave Research Group, University of Malaya, Malaysia. He has published over 20 peer-reviewed journal articles. His research interests include surface plasmon resonance, dielectric metasurfaces, nanophotonics, optical sensors, and optical devices.

SHILUN FENG is currently pursuing the Ph.D. degree in biomedical engineering with the School of Engineering, Faculty of Science and Engineering, Macquarie University, Australia. His research interests include microfabrication, simulation and modeling, and biodevice and instrumentation systems.

RAJIB AHMED is currently a Postdoctoral Fellow with the Stanford for Cancer Early Detection, School of Medicine, Stanford University, USA. He is also an Active Editor and a Reviewer of a number of journals. He has published over 40 peer-reviewed journal articles. His research interest includes micro- and nano-technologies-based biomedical opto-fluidic devices. He received several prestigious research awards and travel grants.

MOHSEN DORRAKI (M'08) was born in Gorgan, Iran, in 1984. He received the B.Eng. degree in electronics engineering from the Azad University of Birjand, Iran, in 2007, and the M.Sc. degree in electrical engineering from the Amirkabir University of Technology, Tehran, Iran, in 2011. He is currently pursuing the Ph.D. degree with the School of Electrical and Electronic Engineering, The University of Adelaide, Adelaide, Australia.

His current research interests include deep learning, signal processing, and biomedical engineering. He received the ECMS Divisional Scholarship from The University of Adelaide for his Ph.D. degree under the supervision of D. Abbott, A. Allison, and B. J. Coventry, in 2017.

ALEX DINOVITSER (M'18) is currently a Postdoctoral Fellow with The University of Adelaide, Australia. He has worked within the electronics manufacturing industry, designing computer interface and signal acquisition systems. In 2008, he built the first spectroscopic LiDAR in Australia for the differential absorption detection of atmospheric trace gasses. He is also a member of the Optical Society of America (OSA) and Engineers Australia.

BRIAN WAI-HIM NG is currently a Senior Lecturer with the School of Electrical and Electronic Engineering, The University of Adelaide. His research interests include radar signal processing, wavelets and terahertz (T-ray) signal processing. He is also an Active Member within the South Australian Chapter of the IEEE. He was awarded the University of Adelaide Medal for the Top Graduate in Electrical and Electronic Engineering.

DEREK ABBOTT (M'85–SM'99–F'05) was born in London, U.K., in 1960. He received the B.Sc. degree (Hons.) in physics from Loughborough University, Loughborough, U.K., in 1982, and the Ph.D. degree in electrical and electronic engineering from The University of Adelaide, Adelaide, SA, Australia, in 1995, under the supervision of K. Eshraghian and B. R. Davis. His research interests include the area of multidisciplinary physics and electronic engineering applied to complex systems. His research programs span a number of areas of stochastics, game theory, photonics, biomedical engineering, and computational neuroscience. He is a Fellow of the Institute of Physics, U.K. He received a number of awards, including the South Australian Tall Poppy Award for Science, in 2004, the Premier's SA Great Award in Science and Technology for outstanding contributions to South Australia, in 2004, an Australian Research Council Future Fellowship, in 2012, the David Dewhurst Medal, in 2015, the Barry Inglis Medal, in 2018, and the M. A. Sargent Medal, in 2019. He has served as an Editor and/or a Guest Editor for a number of journals, including the IEEE JOURNAL OF SOLID-STATE CIRCUITS, *Journal of Optics B*, *Microelectronics Journal*, *Chaos*, *Smart Structures and Materials*, *Fluctuation and Noise Letters*, the PROCEEDINGS OF THE IEEE, and the IEEE PHOTONICS JOURNAL. He is currently on the editorial boards of *Scientific Reports* (Nature), *Royal Society Online Science*, and *Frontiers in Physics*. He is also the Editor-in-Chief (EIC) of IEEE ACCESS.